Solvothermal syntheses, characterizations and properties of three transition metal (Ni(II), Co(II)) imino-carboxylate-diphosphonates†

Kuirong Ma,[ab] Jianing Xu,[a] Lirong Zhang,[a] Jing Shi,[a] Daojun Zhang,[a] Yulan Zhu,[b] Yong Fan*[a] and Tianyong Song*[a]

Received (in Gainesville, FL, USA) 13th August 2008, Accepted 18th December 2008
First published as an Advance Article on the web 12th February 2009
DOI: 10.1039/b814080d

Three compounds have been isolated from solvothermal reactions of a transition metal(II) (Ni(II), Co(II)) with *N*,*N*-bis(phosphonomethyl)aminoacetic acid [$(HO_2CCH_2)N(CH_2PO_3H_2)_2$] ($H_5L$), namely $[NH_3(CH_2)_3NH_3](NH_4)_4[Ni(L)(H_2O)]_2$ (**1**), $(H_3O)_3[Ni(L)(H_2O)_2]\cdot 4H_2O$ (**2**) and $(H_3O)[Co(H_2L)(H_2O)_2]\cdot 2H_2O$ (**3**). These compounds were characterized by single crystal and powder X-ray diffraction, infrared spectroscopy, thermal analysis, elemental analysis, fluorescent spectroscopy and magnetic measurements. The structure of compound **1** is composed of binuclear $[Ni_2O_6N_2]_n^{4-}$ units, which are further interconnected into a 3D supramolecular network by hydrogen bonds. Compounds **2** and **3** are both mononuclear and consist of similar octahedral $[MO_5N]$ units. A 1D dendritic water chain is formed by hydrogen bond interactions in the supramolecular network of compound **2**. Compounds **1** and **2** show ferromagnetic properties, while weak antiferromagnetic properties are observed in compound **3**. Compounds **1** and **2** also display fluorescent emission excited at 235 nm.

Introduction

In recent years, metal phosphonates have been synthesized due to their novel, fascinating architectures and potential applications in catalysis, proton conductivity, ion exchange, optical properties and materials chemistry.[1,2] One promising field is the synthesis of metal phosphonates functionalized with carboxylic, amino or amino-carboxylic groups. Phosphonic acids with additional carboxylic functional groups are useful ligands for the structural construction of inorganic–organic hybrid compounds because the introduction of carboxylic groups does not only provide additional coordination sites, but also increases the solubility of the resulting metal phosphonates and facilitates their crystallization.[1d,3d] Metal(II) phosphonates based on phosphonic acid-containing multifunctional groups are continuing to increase in number.

N,*N*-Bis(phosphonomethyl)aminoacetic acid (H_5L), which has a carboxylic group, two phosphonic acid groups and a central N-donor atom (three types of functional group), is a versatile ligand that can adopt various kinds of coordination mode under different reaction conditions. The resulting metal derivatives have been found to form 1D, 2D and 3D structures, some of which are supramolecular frameworks.[3] Only nine compounds had been synthesized by hydrothermal[4] or conventional solution[3a,b] methods based on a Cambridge Structure Database (CSD) (August, 2008) search until now.[5] In particular, low-dimensional metal imino-carboxylate-diphosphonates based on H_5L, containing water chains, have been rarely reported. Mao *et al.* have reported five 2D (Zn(II), Co(II), Pb(II), La(III)) and three zero-dimensional (Ni(II), Co(II)) metal diphosphonates with the ligand H_5L by chelation in tetradentate mode.[4] The majority of the aforementioned materials were isolated from hydrothermal and conventional solution reactions, and only a few of them were prepared by solvothermal methods during the synthesis process.[3c,d] Currently, our research is focused on the synthesis of novel low-dimensional metal diphosphonates with interesting magnetic properties from H_5L and transition metals by using solvothermal methods and weak acidic reaction conditions. Herein, we report the synthesis, crystal structure and characterization of three new metal imino-carboxylate-diphosphonates: dimer $[NH_3(CH_2)_3NH_3](NH_4)_4[Ni(L)(H_2O)]_2$ (**1**), and mononuclear compounds $(H_3O)_3[Ni(L)(H_2O)_2]\cdot 4H_2O$ (**2**) and $(H_3O)[Co(H_2L)(H_2O)_2]\cdot 2H_2O$ (**3**) from solvothermal reactions using organic amines or ammonium salts as structure-directing agents. The luminescent and magnetic properties of these compounds are reported herein.

Experimental section

Materials and methods

All chemicals were obtained from commercial sources and used without further purification. Elemental analyses were conducted using a Perkin-Elmer 2400 LC II elemental analyzer. IR spectra were obtained using a Nicolet Impact 410 FI-IR spectrometer with KBr pellets in the 400–4000 cm^{-1} region. Thermogravimetric analyses (TGA) were performed in an atmospheric environment with a heating rate of 10 °C min^{-1}

[a] *State Key Laboratory of Inorgnic Synthesis and Preparative Chemistry, College of Chemistry, Jilin University, Changchun, Jilin, P R China. E-mail: mrfy@jlu.edu.cn*
[b] *Jiangsu key laboratory for chemistry of low-dimensional materials, Department of Chemistry, Huaiyin Teachers College, Huaian, Jiangsu, P R China*

† Electronic supplementary information (ESI) available: Further spectra, crystal structure pictures and crystallographic details. CCDC 610098, 610099 and 629612. For ESI and crystallographic data in CIF or other electronic format see DOI: 10.1039/b814080d

using a Perkin-Elmer TGA 7 thermogravimetric analyzer. Magnetic susceptibility data were collected, respectively, on 0.1167 g (**1**), 0.0473 g (**2**) and 0.0169 g (**3**) of sample in the temperature range 4–300 K in a magnetic field of 1 kOe using a Quantum Design MPMS-7 SQUID magnetometer. Emission and excitation spectra were recorded using an Eidingberg FX 900 photoluminescent spectrometer with a 500 W xenon lamp. Emission spectra were corrected for the sensitivity of the photomultiplier tube, and excitation spectra were corrected for the intensity of the xenon lamp. Powder X-ray diffraction (XRD) patterns were collected on an ARL X'TRA diffractometer using graphite-monochromated Cu-K_α radiation (λ = 1.5418 Å) in the angular range 2θ = 4–40° with a stepping size of 0.02° and a counting time of 4 s per step.

Syntheses

The preparation of {[$NH_3(CH_2)_3NH_3$][$(NH_4)_4$}[Ni(L)(H_2O)]$_2$ (1). A mixture of $NiCl_2{\cdot}6H_2O$ (0.19 g, 0.8 mmol), H_5L (0.21 g, 0.8 mmol) and NH_4F (0.075 g, 2.0 mmol) were dissolved in 10 mL ethanol. 1,3-Propyldiamine (1,3-PDA) was added into the above mixture, which was then sealed into an autoclave equipped with a 15 mL PTFE-lined stainless steel vessel and heated at 170 °C for 5 d. Green crystals of compound **1** were collected by vacuum filtration, washed thoroughly with ethanol and dried in air (yield 62% based on nickel). Elemental analysis ($Ni_2C_{11}N_8H_{44}O_{18}P_4$): C, 16.15; H, 5.38; N, 13.69. Calc.: C, 16.07; H, 5.33; N, 13.54%. IR data (/cm^{-1}): 3365 (ms), 3206 (ms), 2119 (w), 1608 (s), 1531 (w), 1490 (w), 1392 (ms), 1338 (w), 1249 (ms), 1108 (s), 1056 (s), 985 (ms), 862 (w), 732 (ms), 603 (ms) and 491 (w).

The preparation of [$(H_3O)_3$][Ni(L)(H_2O)$_2$]·$4H_2O$ (2). The synthesis was similar to that described for **1**. Tetramethylammonium hydroxide (TMAOH, 2.0 mmol, 15% V/V) was added into the above mixture, which was then sealed into an autoclave equipped with a 15 mL PTFE-lined stainless steel vessel and heated at 170 °C for 5 d. Green crystals of compound **2** were collected by vacuum filtration, washed thoroughly with ethanol and dried in air (yield 46% based on nickel). Elemental analysis ($NiC_4NH_{27}O_{17}P_2$): C, 10.05; H, 5.72; N, 3.09. Calc.: C, 9.96; H, 5.62; N, 2.92%. IR data (/cm^{-1}): 3208 (vs), 1589 (s), 1430 (s), 1251 (w), 1049 (s), 937 (ms), 736 (ms), 607 (w) and 484 (w).

The preparation of (H_3O)[Co(H_2L)(H_2O)$_2$]·$2H_2O$ (3). The synthesis was similar to that described for **2**, except for using $CoCl_2{\cdot}6H_2O$ (0.19 g, 0.8 mmol) instead of $NiCl_2{\cdot}6H_2O$. Pink crystals of compound **3** were collected by vacuum filtration, washed thoroughly with ethanol and dried in air (yield 52% based on cobalt). Elemental analysis ($CoC_4NH_{19}O_{13}P_2$): C, 12.03; H, 4.76; N, 3.57. Calc.: C, 11.91; H, 4.63; N, 3.51%. IR data (/cm^{-1}): 3220 (vs), 1602 (s), 1440 (s), 1328 (w), 1257 (ms), 1106 (s), 939 (s), 802 (w), 728 (s), 597 (s), 563 (ms) and 443 (ms).

Crystallography

Single crystals of **1–3** were mounted on a Siemens Smart CCD diffractometer equipped with graphite-monochromated Mo-K_α radiation (λ = 0.71073 Å). Intensity data were collected at 293 ± 2 K and processed on a PC using the SAINT Plus software package. All structures were solved by direct methods and refined by full-matrix least-squares fitting on F^2 using the SHELXTL-97 software package.[6] All non-hydrogen atoms were refined with anisotropic thermal parameters. The positions of the hydrogen atoms were either located by difference Fourier maps or calculated geometrically, and their contributions to structural factor calculations included.† The crystallographic data and structural refinements are summarized in Table 1. Selected bond lengths (Å) and angles (°) of **1–3** are list in Table S1 (see ESI†). The hydrogen bond lengths (Å) and angles (°) of **1–3** are given in Table S2 (see ESI†).

Results and discussion

The effect of different organic solvents, including ethanol, tetrahydrofuran (THF), ethylene glycol (EG) and 1-butanol, on crystal quality has been investigated. The results show that only ethanol is suitable for preparing high quality crystals. However, under similar conditions, for EG, the obtained product is a powder, for THF, a clear solution and, for 1-butanol, a semi-transparent solid grain. The may result from the dielectric constant (ε), boiling point (b.p.) or polarity of the solvent, *etc*. The boiling point of THF is 66 °C, of ethanol is 78 °C, of 1-butanol is 118 °C and of EG is 198 °C, respectively, and their ε values are 7.52, 24.3, 17.8 and 37, respectively. In general, solvents with a low boiling point and a small dielectric constant are more desirable for crystallization under solvothermal conditions.[7] Accordingly, THF and ethanol should be the better candidates. However, THF is undesirable for crystallization in this case (according to the rule of dielectric constants, THF belongs to the class of ring-shaped ethers and can be regarded as a non-polar solvent, but ethanol is a polar solvent).

We also investigated the effect of organic amine and ammonium salts on the crystallization under solvothermal conditions. NH_4F was used in the synthesis, yet the compounds do not contain F^-, even though it is crucial to the synthesis by acting as a mineralizing agent. Apart from NH_4F, 1,3-PDA and TMAOH have also been employed during the aforementioned reactions. The results reveal that the structure of the final product is affected by the organic amine and/or ammonium salt that acted as the structure-directing agent. The size and conformation of the organic amine and ammonium salt play an important role in the synthesis process: using larger sized organic amines as templates, low-dimensional multinuclear compounds tend to be obtained. Herein, binuclear compound **1** was synthesized by employing 1,3-PDA, and mononuclear compounds **2** and **3** were obtained by using smaller sized TMAOH.

Description of the structures

The crystal structure of {[$NH_3(CH_2)_3NH_3$][$(NH_4)_4$}[Ni(L)(H_2O)]$_2$ (1). As shown in Fig. 1a, the asymmetric unit of **1** contains one Ni(II) ion, one L ligand, one protonated 1,3-PDA cation, one water ligand and two NH_4^+ cations. The Ni(II) is surrounded by five oxygen atoms and one nitrogen atom, in which three oxygen atoms (O1, O4, O7) and one nitrogen

Table 1 Crystallographic data and refinement details for compounds **1–3**

Compound	**1**	**2**	**3**
Empirical formula	$C_{11}H_{44}N_8Ni_2O_{18}P_4$	$C_4H_{27}NNiO_{17}P_2$	$C_4H_{19}NCoO_{13}P_2$
Formula weight	817.84	481.92	410.07
Temperature/K	293(2)	293(2)	293(2)
Crystal system	Monoclinic	Monoclinic	Triclinic
Space group	C_2/c	$P2_1/n$	$P\bar{1}$
a/Å	11.315(2)	11.568(2)	9.3817(2)
b/Å	19.282(4)	10.689(2)	9.3988(2)
c/Å	14.432(3)	15.816(3)	9.776(2)
α (°)	90	90	82.84(3)
β (°)	103.01(3)	109.17(3)	62.55(3)
γ (°)	90	90	76.32(3)
Volume/Å^3	3067.8(1)	1847.2(6)	743.2(3)
D_{calc}/g cm^{-3}	1.771	1.733	1.833
Z	4	4	2
μ/mm^{-1}	1.522	1.305	1.435
Reflections collected	15025	17748	7382
Unique reflections	3526	4226	3405
R_{int}	0.0378	0.0354	0.0167
GOF on F^2	1.094	1.055	1.045
R_1 $[I > 2\sigma(I)]^a$	0.0302	0.0376	0.0315
wR_2 $[I > 2\sigma(I)]^b$	0.0682	0.0925	0.0877
R_1 (all data)^a	0.0361	0.0444	0.0342
wR_2 (all data)^b	0.0710	0.0959	0.0897

^{a} $R_1 = \Sigma||F_o| - |F_c||/\Sigma|F_o|$. ^{b} $wR_2 = \{\Sigma[w(F_o^2 - F_c^2)^2]/\Sigma[w(F_o^2)]^2\}^{\frac{1}{2}}$.

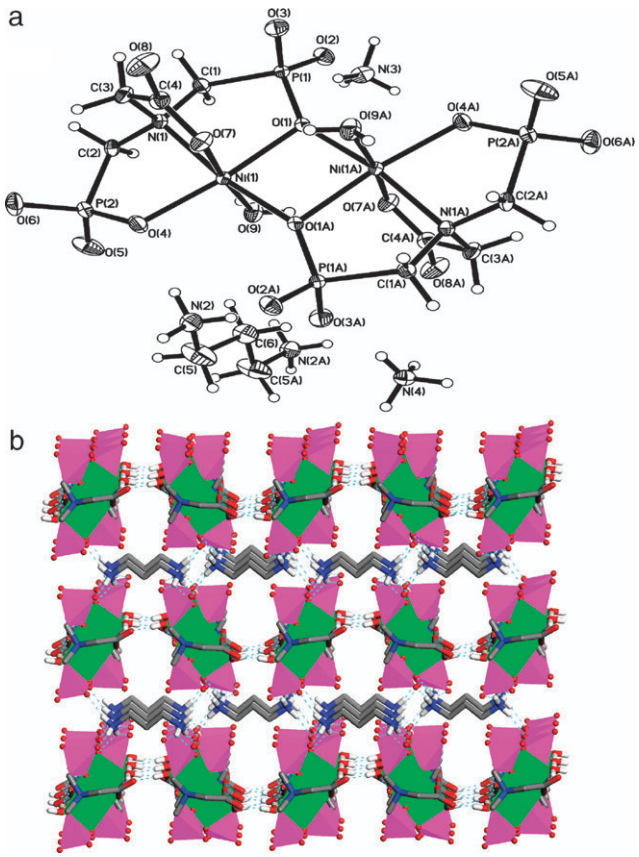

Fig. 1 (a) An ORTEP diagram showing the dimer structure of **1** with 30% probability ellipsoids. (b) The 3D O–H···N (1,3-PDA) hydrogen-bonded network of **1** in the ab plane. Hydrogen bonds are drawn as dotted blue lines and NH_4^+ ions are omitted for clarity.

(N(1)) atom are from one L ligand, one oxygen atom (O1A) comes from the adjacent L ligand and the last oxygen (O(9)) is from a coordinated water molecule. The Ni(II) center has a slightly distorted octahedral geometry, with a shared position (O(1)) being occupied by a μ_2-phosphonate group [Ni–O(1)–Ni]. The Ni(1)–O(N) distances range from 2.0371(2) to 2.103(2) Å and the O–Ni(1)–O and O–Ni(1)–N angles range from 84.33(8) to 174.21(8)°, deviating from the values of an ideal octahedron. These bond lengths and angles are similar to those of other Ni(II) phosphonates.[4b]

Compound **1** exhibits a 3D supramolecular network constructed from dimeric units $[Ni_2O_6N_2]$ through hydrogen bonds. Two Ni(II) ions are bridged by a phosphonate oxygen (μ_2-O(1)), resulting in the formation of a dimeric unit $[Ni_2O_6N_2]$ with a Ni···Ni distance of 3.056 Å. These binuclear units are further interconnected with each other *via* O–H···O hydrogen bonds between the carboxylate oxygen (O(8)) and the coordinated water (O(9)), resulting in a 1D double chain along the c axis (Fig. SA1, see ESI†). The O(8)–H(2)···O(9) distance is 2.732(3) Å and the bond angle is 171(3)°. Many O–H···N hydrogen bonds are formed by the 1,3-PDA (N(2), N(2A) cations, NH_4^+ (N(3), N(4)) cations and uncoordinated oxygen atoms (O(2), O(3), O(4), O(5), O(6)). Consequently, a 3D supramolecular network (Fig. 1b; Fig. SA2, see ESI†) is created by hydrogen bonding.

The crystal structure of $[(H_3O)_3][Ni(L)(H_2O)_2]\cdot 4H_2O$ (2). The asymmetric unit of **2** (Fig. 2a) consists of 25 non-hydrogen atoms: one Ni(II) atom, two P atoms, one N atom, four C atoms, ten framework O atoms and seven non-framework O atoms. The Ni(II) ion is six-coordinate, with two water ligands (O(9), O(10)) and one L moiety. The H_5L ligand acts as a tetradentate ligand, providing two oxygen atoms (O(1), O(4)) from the $-PO_3$ group, one nitrogen atom (N(1)) and one carboxylate oxygen (O(7)) atom to chelate with Ni(1). The distances Ni(1)–N(1), Ni(1)–O(1), Ni(1)–O(4), Ni(1)–O(7), Ni(1)–(O9) and Ni(1)–O(10) are 2.115(2), 2.0866(18),

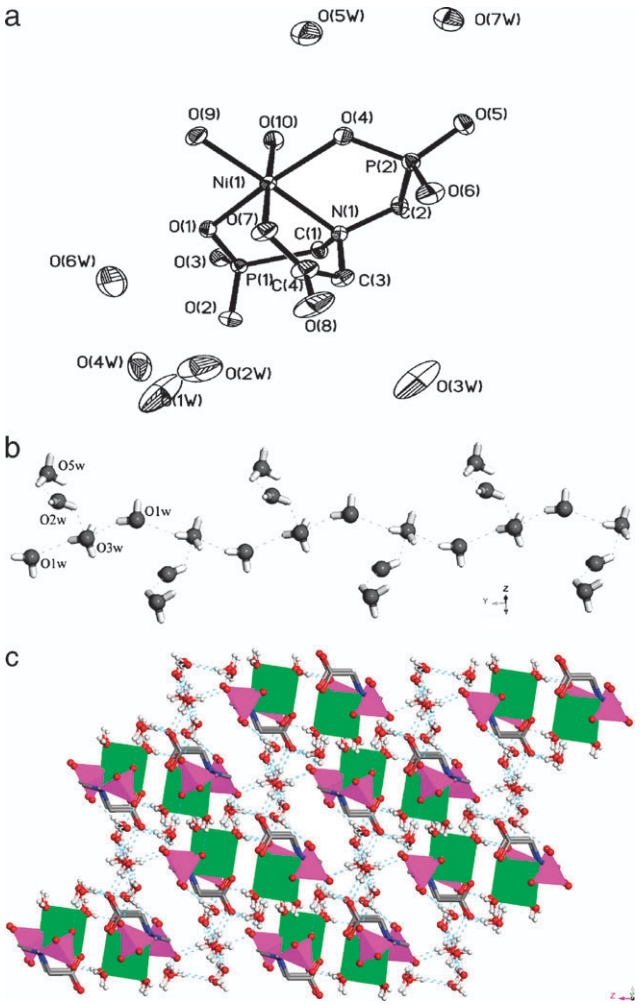

Fig. 2 (a) An ORTEP diagram showing the mononuclear structure of **2** with 50% probability ellipsoids. (b) The 1D O–H···O hydrogen-bonded dendritic water chain of **2** along the a axis. Hydrogen bonds are drawn as dotted lines. (c) The 3D network built by hydrogen bonds from the water chains of **2**. Hydrogen bonds are drawn as dotted blue lines.

2.1246(19), 2.038(2), 2.042(2) and 2.0550(8) Å, respectively. The O–Ni(1)–O bond angles range from 87.28(8) to 178.23(8)°, which indicates that each [NiO_5N] unit adopts a distorted octahedral coordination geometry. These distances and angles are generally consistent with those of other Ni(II) phosphonates.[4b]

Considering the charge balance of the coordination environment, the O–H distance of the lattice water molecules and their acidic environment, three of the lattice water molecules (O(3w), O(5w), O(6w)) are protonated.

The [NiO_5N] octahedra, as the basic structure unit, are connected to each other running along the b axis *via* hydrogen bonds formed by coordinated water oxygen atoms O(9) and phosphonate oxygen atoms O(6), creating a 1D chain (Fig. SA3, see ESI†). The O(9)···O(6) distance is 2.730(3) Å and the bond angle is 168(4)°. 2D layers (Fig. SA4, see ESI†) are constructed from these 1D chains *via* hydrogen bonds O(9)···O(6), O(9)···O(3) and O(10)···O(1) in the ac plane (Fig. SA4). The O(9)···O(3) and O(10)···O(1) bond distances and angles are 2.730(3) and 2.714(3) Å, and 168(4) and 175(4)°, respectively.

A dendritic water chain is built from hydrogen bonds among the water molecules O(1w), O(2w), O(3w) and O(5w) along the a axis, as shown in Fig. 2b. In the dendritic chain, the branches are made up of O(1w) and O(3w), and the leaves of O(2w) and O(5w).

2D layers are also constructed by hydrogen bonds from water chains in the bc plane (Fig. SA5, see ESI†). As shown in Fig. 2c, hydrogen bonds further extend the structure into a 3D supramolecular network. The O(1w)···O(3w), O(3w)···O(2w) and O(2w)···O(5w) bond distances and angles are 3.035(6), 2.774(1) and 3.055 Å, and 152(5), 102(6) and 126(3)°, respectively.

The crystal structure of $(H_3O)[Co(H_2L)(H_2O)_2]\cdot 2H_2O$ (3). As shown in Fig. 3a, the coordination environment of **3**, having mononuclear $[Co(H_2L)(H_2O)_2]_n^-$ anions, strongly resembles that of **2**; the Co(II) atom is also six-coordinated by oxygen atoms. The ligand H_2L acts as tetradentate ligand, providing two phosphonate oxygen atoms (O(3), O(6)), one nitrogen atom (N(1)) and one carboxylate oxygen atom (O(2)). The Co(1)–N and Co(1)–O bond distances range from 2.0513(2) to 2.183(2) Å, and the O–Co(1)–O(N) angles range from 88.46(9) to 179.01(8)°, deviating from the values for an ideal octahedron but consistent with those of other Co(II) phosphonates.[3c]

Taking into account the charge balance and their acidic environment, the phosphonate oxygen atoms (O(7), O(8)) and lattice water molecule (O(10)) are protonated, based on the long P–O and O–H distances, which differ from those of compound **2**.

The [CoO_5N] octahedrons, as the basic structure unit, are interconnected *via* hydrogen bonds into 1D chains along the

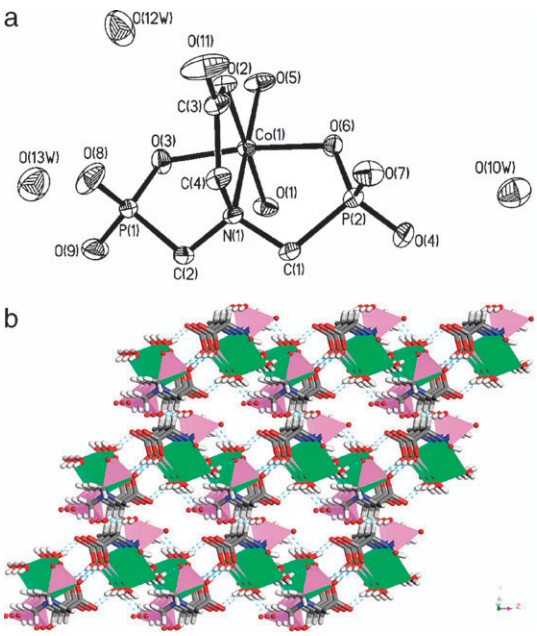

Fig. 3 (a) An ORTEP diagram showing the mononuclear structure of **3** with 50% probability ellipsoids. (b) The 3D O–H···O hydrogen-bonded network of **3**. Hydrogen bonds are drawn as dotted blue lines. Lattice water molecules are omitted for clarity.

b axis (Fig. SA6, see ESI†), and are identical to those of compound **2**. These 1D chains stack up to form 2D layers *via* hydrogen bonds along the ab and bc plane, respectively (Fig. SA7 and Fig. SA8, see ESI†). Thus, a 3D supramolecular network (Fig. 3b) is built from these 2D layers *via* hydrogen bonds formed by coordinated water molecules (O(1), O(5)), and uncoordinated phosphonate oxygen (O(4), O(6), O(9)) and uncoordinated carboxylate oxygen (O(11)) atoms. Hydrogen bonds formed by the lattice water molecules (O(10w), O(12w), O(13w)) and the uncoordinated phosphonate oxygen atoms (O(3), O(4), O(7), O(8), O(9)) further reinforce the framework.

XRD and IR characterization

The experimental data for compounds **1–3** (Fig. SB1–3, see ESI†) are in good agreement with the simulated XRD powder patterns based on single crystal data X-ray diffraction analysis, indicating the phase purity of the as-synthesized samples.

IR spectra of the three compounds were recorded in the 4000 to 400 cm^{-1} region (Fig. SC1–3, see ESI†). The band centred at 3365 cm^{-1} for **1** could be assigned to N–H stretching vibrations, and the bands located at 3149 and 3076 cm^{-1} could be assigned to O–H stretching vibrations of the coordinated water molecule. The asymmetric and symmetric stretching vibrations of the carboxyl group are centred at 1608 cm^{-1}, and 1419 and 1392 cm^{-1}, respectively. The bands at 1249 and 1108 cm^{-1}, and 1056 and 985 cm^{-1}, can be attributed to the vibrations of the P═O and P–O group, respectively. For compound **2**, the bands centred at 3326 and 3205 cm^{-1} could be assigned to the O–H stretching vibrations of the protonated water, lattice water and coordinated water molecules. The asymmetric and symmetric stretching vibrations of the carboxyl group are centred at 1589 cm^{-1}, and 1430 and 1401 cm^{-1}, respectively. The bands at 1245 and 1078 cm^{-1}, and 1049 and 973 cm^{-1}, can be attributed to the vibrations of the P═O and P–O group, respectively. For compound **3**, the bands centred at 3423 and 3220 cm^{-1} could be assigned to the O–H stretching vibrations of the protonated water, lattice water and coordinated water molecules, and the PO–H groups. The asymmetric and symmetric stretching vibrations of the carboxyl group are centred at 1602 and 1440 cm^{-1}, respectively. The bands at 1261 cm^{-1}, and 1106 and 939 cm^{-1}, can be attributed to the vibrations of the P═O and P–O group, respectively.

Thermogravimetric studies

The TGA curves of **1–3** are shown in Fig. SD (see ESI†). The TGA curve of compound **1** consists of two weight losses. The first loss of 20.0% starts at 250 °C, owing to the release of the two water ligands, one protonated 1,3-PDA cation, four NH_4^+ cations and the pyrolysis of the organic ligands (calc. 20.3%), and is complete at about 385 °C. The second loss of 49.2%, between 385 and 1000 °C, can be attributed to the weight loss of the organic component. The final residue is mainly $Ni(PO_3)_2$. The TGA curve of compound **2** exhibits two major weight losses. The first weight loss of 34.1% starts at 65 °C and continues up to 340 °C, owing to the release of lattice water molecules and water ligands (calc. 34.2%). The second process, from 340 to 1000 °C, can be assigned to the pyrolysis of the organic ligand. The total weight loss is 67.4%, consistent with the calculated value of 69.5%, and the final residue is mainly NiO. There are two main steps of weight loss for compound **3**. The first loss of about 13.3%, occurring in the region 120–230 °C, corresponds to the loss of three lattice water molecules (calc. 13.4%). The second loss of 52.9%, in the region 230–1000 °C, corresponds to the loss of two water ligands and two water molecules from the condensation of the phosphonate groups and the decomposition of the phosphonate ligand (calc. 52.9%). The final residue is mainly $Co(PO_3)_2$.

Magnetism properties

The magnetic susceptibilities of compounds **1–3** in the solid state were measured in the temperature range from 4 to 300 K at an applied magnetic field of 1 kOe. The temperature dependence of the molar magnetic susceptibility, together with its corresponding $\chi_m T$ product, for compounds **1–3** is shown in Fig. 4a–c, respectively.

$\{[NH_3(CH_2)_3NH_3](NH_4)_4\}[Ni(L)(H_2O)]_2$ (1). The $\chi_m T$ value of **1** gradually increased with cooling up to a maximum of 3.4 emu K mol^{-1} at 7 K (Fig. 4a), indicating a ferromagnetic interaction between the Ni(II) ions. Upon further decreasing the temperature, the $\chi_m T$ value rapidly reduced, which could mainly be caused by spin–orbit couplings. The observed $\chi_m T$ value of 2.40 emu K mol^{-1} at 300 K is close to the expected value for two isolated Ni(II) centers ($S = 1$, $g = 2.2$). The fit of the magnetic data above 7 K was done using the Curie–Weiss law $\chi_m = C_m/(T - \theta)$: $C = 2.37$ emu K mol^{-1} and $\theta = 5.91$ K. The positive θ value was further confirmed by the weak ferromagnetic interaction between the Ni(II) ions.

Compound **1** is a dimer with a Ni···Ni distance of 3.056 Å and a Ni–O–Ni angle of 95.4°. This angle is within the range of (90 ± 14)° suggestive for ferromagnetic coupling.[8] The nearest interdimer Ni···Ni distance is 7.375 Å, which is very unfavorable for super-exchange between metal centers. Therefore, coupling exchange interactions between dimers are negligible and the main role of the coupling occurs within dimer molecules.

The magnetic susceptibility data were fitted to an exchange expression[9] containing a Weiss-like temperature correction term, θ, for interdimeric exchange (eqn (1)) based on the appropriate isotropic Heisenberg Hamiltonian $H = -2JS_1S_2$, in which J is the coupling constant:[10]

$$\chi_m = \frac{N\mu_B^2 g^2}{3k(T-\theta)} \times \frac{5 + \exp(-4x)}{5 + 3\exp(-4x) + \exp(-6x)} \qquad (1)$$

where $x = J/kT$, and J, N, g, μ_B and k have their usual meanings. Best fit results were obtained: $2J = +9.37$ cm^{-1}, $g = 2.17$ and $\theta = -0.35$ K. The negative θ value indicates that the interdimeric interactions are antiferromagnetic at low temperature.

$[(H_3O)_3][Ni(L)(H_2O)_2]\cdot 4H_2O$ (2). The plot of $\chi_m T$ (Fig. 4b) for **2** shows that the $\chi_m T$ value increases to a maximum of 1.27 emu K mol^{-1} at 40 K upon cooling, representing the

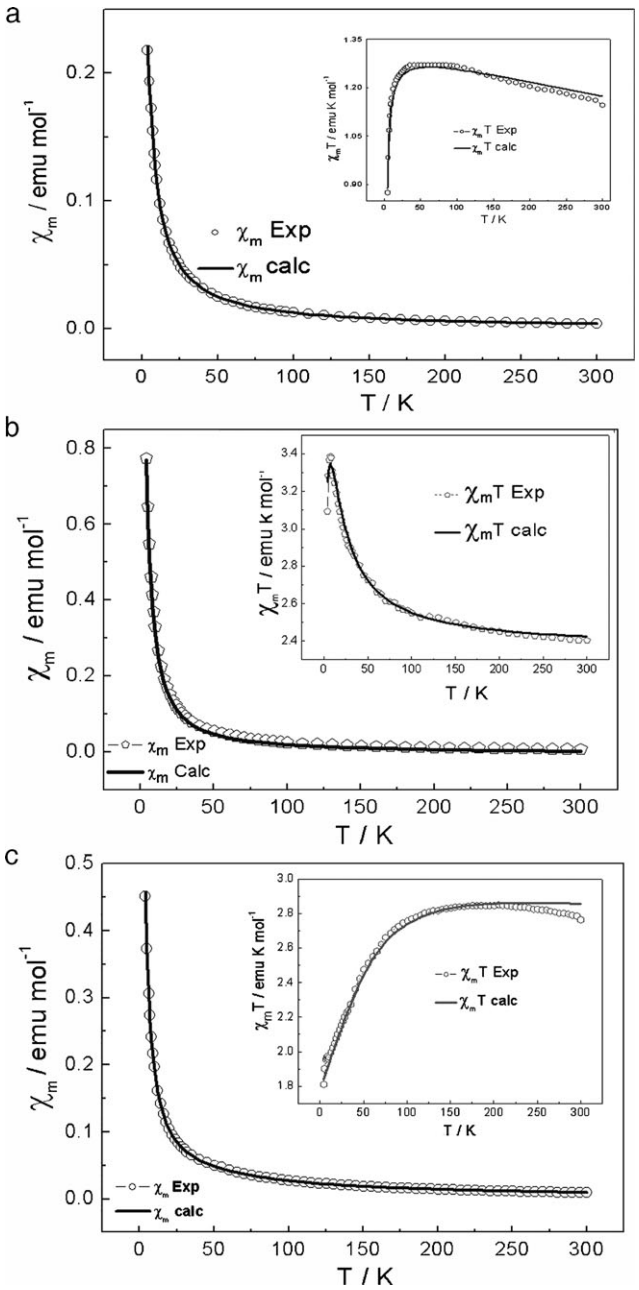

Fig. 4 (a) The temperature dependence of χ_m and $\chi_m T$ for (a) **1**, (b) **2** and (c) **3**. The solid lines show the fitting results.

presence of ferromagnetic coupling between the Ni(II) ions. The $\chi_m T$ value decreases rapidly upon cooling below 40 K. The experimental data were fitted to the Curie–Weiss equation above 40 K, with $C = 1.13$ emu K mol^{-1} and $\theta = 10.67$ K. At room temperature, the observed $\chi_m T$ value was 1.15 emu K mol^{-1}, close to the expected value of 1.2 emu K mol^{-1} for an isolated Ni(II) ion ($S = 1$, $g = 2.2$).

The magnetic susceptibility data were fitted to an isolated Ni(II) ion with a ZFS effect (D). The spin Hamiltonian used was as follows:

$$H = g\mu_B HS + D\left[S_z^2 - \frac{S(S+1)}{3}\right]. \quad (2)$$

Eqns (3)–(7) for the magnetic susceptibility of this system were valid for obtaining the best fit:

$$\chi_{11} = \frac{2Ng_z^2\mu_B^2}{k_B T} \times \frac{e^{-x}}{1+2e^{-x}} \quad (3)$$

$$\chi_{\perp} = \frac{2Ng_x^2\mu_B^2}{D} \times \frac{1-e^{-x}}{1+2e^{-x}} \quad (4)$$

where $x = D/k_B T$, g_z and g_x are the Landé factors associated with the z- and x-directions, and D is the crystal field splitting. Within this approximation, the model includes the influence of the orbital momentum for spin–orbit coupling and ligand field distortions. The average molar magnetic susceptibility for a powder sample is given by the well-known relationship:[11]

$$\chi_{Ni} = \frac{\chi_{11} + 2\chi_{\perp}}{3} + \text{TIP}. \quad (5)$$

$$\chi_{Ni(II)} = \frac{2Ng_z^2\mu_B^2}{3} \times \left(\frac{\exp(-x)}{k_B T(1+2\exp(-x))}\right) + \frac{2Ng_x^2\mu_B^2}{3} \times \frac{2(1-\exp(-x))}{D(1+2\exp(-x))} + \text{TIP} \quad (6)$$

Considering the intermolecular interaction, the mean-field approximation was treated:[12]

$$\chi_m = \frac{\chi_{Ni}}{1 - \left(\frac{2zJ'}{Ng^2\mu_B^2}\right)\chi_{Ni}}. \quad (7)$$

The best parameters, based on eqn (7), were $g = 2.30$, $D/k_B = +5.04$ K, TIP $= -4.8 \times 10^{-4}$ emu mol^{-1} and $zJ'/k_B = -1.4$ K, respectively. The zJ' term is a Weiss-like temperature correction term, indicating the intermolecular interaction. The TIP term corresponds here to a diamagnetic correction.

$(H_3O)[Co(H_2L)(H_2O)_2]\cdot 2H_2O$ (3). For compound **3**, the $\chi_m T$ *vs.* temperature plot (Fig. 4c) is close to a constant value of 2.84 emu K mol^{-1} from room temperature to 120 K, which is obviously larger than the spin-only value of 1.875 emu K mol^{-1} for a Co(II) ion ($S = \frac{3}{2}$, $g = 2.00$) at 300 K. This indicates that the contribution of the spin–orbit coupling and the distortion of the octahedral crystal field cannot be neglected.[11,13] From 100 to 50 K, the $\chi_m T$ value drops smoothly and below 50 K drops sharply to a value of 1.96 emu K mol^{-1} at 9 K. Below 9 K, the $\chi_m T$ value increases slightly, which suggests the onset of magnetic order,[13] and finally decreases to a value of 1.81 emu K mol^{-1} at 4 K, which could mainly be caused by spin–orbit coupling.

The magnetic susceptibility data could be fitted to the Curie–Weiss law: $\chi_m = C_m/(T-\theta)$. The results obtained were $C = 2.88$ emu K mol^{-1} and $\theta = -5.4$ K, in which the negative θ value is in agreement with the presence of antiferromagnetic interactions.

For compound **3**, the equation reflecting the magnetic susceptibility of a mononuclear Co(II) ion with spin–orbit

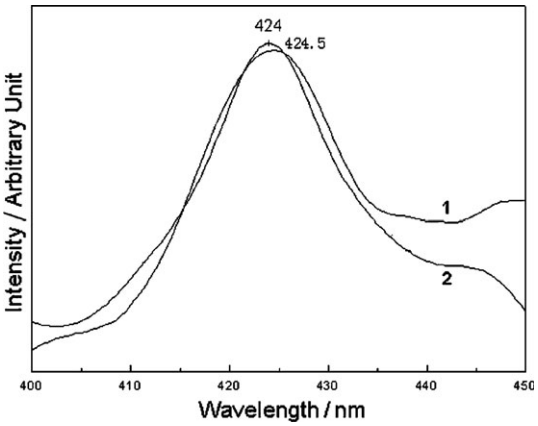

Fig. 5 The solid-state fluorescence emission spectra of compounds **1** and **2** at room temperature excited at 235 nm.

coupling and ligand field distortions in a molecular field approximation[11,14,15] is written as:

$$\chi_{\mathrm{Co(II)}} = \frac{Ng_z^2\mu_B^2}{k_BT} \times \left(\frac{1}{3} \times \frac{1+9\exp(-2x)}{4(1+\exp(-2x))}\right) + \frac{2}{3} \times \frac{Ng_x^2\mu_B^2}{k_BT} \times \frac{1+(3/4x)[1-\exp(-2x)]}{1+\exp(-2x)} + \mathrm{TIP} \quad (8)$$

where $2x = D/k_BT$. The obtained parameters based on eqn (1) are: $g = 2.53$, $D/k_B = 84.89$ K and TIP $= -3.8 \times 10^{-4}$ emu mol^{-1}, respectively. It should be noted that the sign of D cannot be determined as neither a negative sign nor a positive sign has any effect on the result.

Fluorescence properties

According to work reported previously, coordination polymers containing the ligand H_5L can exhibit photoluminescent properties.[4c] Here, we investigated the photoluminescent properties of compounds **1–3** at room temperature, as shown in Fig. 5. The free ligand H_5L showed no emission in the visible region, whereas the nickel(II) diphosphonates showed a fluorescent emission band at $\lambda_{em} = 424.5$ nm ($\lambda_{excitation} = 235$ nm) for compound **1** and $\lambda_{em} = 424$ nm ($\lambda_{excitation} = 235$ nm) for compound **2**, which may be due to ligand-to-metal charge transfer (LMCT) or metal-to-ligand charge transfer (MLCT). To the best of our knowledge, these emission bands have never been reported for Ni(II) imino-carboxylate-diphosphonates. Compound **3** didn't display an emission spectrum in the solid-state at room temperature.

Conclusions

We have reported the preparation of three metal imino-carboxylate-diphosphonates containing the ligand *N*,*N*-bis-(phosphonomethyl)aminoacetic acid [$(HO_2CCH_2)N(CH_2PO_3H_2)_2$] ($H_5L$) by a solvothermal technique. Compound **1** displays a 3D supramolecular network based on a dimer through hydrogen bond interactions. Compound **2** is mononuclear and is further interconnected into a 3D supramolecular network by dendritic water chains. Phosphonates containing water chains based on H_5L have rarely been reported. Compound **3** is also mononuclear and is further interconnected into a 3D supramolecular structure by hydrogen bonds. Magnetism data indicate that compound **3** exhibits anti-ferromagnetic interactions between metal centers, while both compounds **1** and **2** have ferromagnetic properties. Moreover, we have investigated the fluorescence properties of these compounds. Our results indicate that both compounds **1** and **2** show a fluorescence emission band. Further investigations of magnetic transition metal phosphonate compounds prepared by solvothermal methods are in progress.

Acknowledgements

We thank Dr Yun-Ling Liu, Dr Cheng-Ling Pan and Dr Guang-Hua Li for revising the manuscript.

References

1 (*a*) E. W. Stein Sr., A. Clearfield and M. A. Subramanian, *Solid State Ionics*, 1996, **83**, 113; (*b*) A. Clearfield, *Curr. Opin. Solid State Mater. Sci.*, 1996, **1**, 268; (*c*) A. Clearfield, Metal Phosphonate Chemistry, in *Progress in Inorganic Chemistry*, ed. K. D. Karlin, John Wiley & Sons, New York, 1998, vol. 47, pp. 371; (*d*) J.-G. Mao, Z.-K. Wang and A. Clearfield, *J. Chem. Soc., Dalton Trans.*, 2002, 4457.
2 (*a*) D. A. Burwell, K. G. Valentine, J. H. Timmermans and M. E. Thompson, *J. Am. Chem. Soc.*, 1992, **114**, 4144; (*b*) P. H. Mutin, G. Guerrero and A. Vioux, *C. R. Chim.*, 2003, **6**, 1153; (*c*) F. A. A. Paz, J. Rocha, J. Klinowski, T. Trindade, F.-N. Shi and L. Mafra, *Prog. Solid State Chem.*, 2005, **33**, 113; (*d*) J.-G. Mao, *Coord. Chem. Rev.*, 2007, **251**, 1493.
3 (*a*) A. Mateescu, C. P. Raptopoulou, A. Terzis, V. Tangoulis and A. Salifoglou, *Eur. J. Inorg. Chem.*, 2006, 1945; (*b*) A. Mateescu, C. Gabriel, R. G. Raptis, P. Baran and A. Salifoglou, *Inorg. Chim. Acta*, 2007, **360**, 638; (*c*) Y. Fan, G.-H. Li, W.-P. Jian, M. Yu, L. Wang, Z.-F. Tian, T.-Y. Song and S.-H. Feng, *J. Solid State Chem.*, 2005, **178**, 2267; (*d*) S. O. H. Gutschke, D. J. Price, A. K. Powell and P. T. Wood, *Angew. Chem., Int. Ed.*, 1999, **38**, 1088.
4 (*a*) J.-G. Mao, Z.-K. Wang and A. Clearfield, *New J. Chem.*, 2002, **26**, 1010; (*b*) J.-L. Song, J.-G. Mao, Y.-Q. Sun, H.-Y. Zeng, R. K. Kremer and A. Clearfield, *J. Solid State Chem.*, 2004, **177**, 633; (*c*) J.-L. Song, H.-H. Zhao, J.-G. Mao and K. R. Dunbar, *Chem. Mater.*, 2004, **16**, 1884; (*d*) S.-F. Tang, J.-L. Song and J.-G. Mao, *Eur. J. Inorg. Chem.*, 2006, 2011.
5 F. H. Allen, *Acta Crystallogr., Sect. B: Struct. Sci.*, 2002, **58**, 380.
6 G. M. Sheldrick, *SHELXTL version 5.1*, Bruker Analytical X-Ray Systems, Madison, WI, 1997.
7 R.-R. Xu and W.-Q. Pang, *Inorganic Synthesis and Preparative Chemistry*, Higher Education Press, Beijing, 2001, pp. 128.
8 K. K. Nanda, L. K. Thompson, J. N. Bridson and K. Nag, *J. Chem. Soc., Chem. Commun.*, 1994, 1337.
9 A. P. Ginsberg and M. E. Lines, *Inorg. Chem.*, 1972, **11**, 2288.
10 T. Koga, H. Furutachi, T. Nakamura, N. Fukita, M. Ohba, K. Takahashi and H. Okawa, *Inorg. Chem.*, 1998, **37**, 989.
11 O. Kahn, *Molecular Magnetism*, Wiley-VCH, New York, 1993.
12 H. Miyasaka, A. Saitoh, S. Yanagida, C. Kachi-Terajima, K.-i. Sugiura and M. Yamashita, *Inorg. Chim. Acta*, 2005, **358**, 3525.
13 H.-L. Sun, Z.-M. Wang and S. Gao, *Inorg. Chem.*, 2005, **44**, 2169.
14 (*a*) F.-N. Shi, F. A. A. Paz, P. Girginova, J. Rocha, V. S. Amaral, J. Klinowski and T. Trindade, *J. Mol. Struct.*, 2006, **789**, 200; (*b*) J.-L. Song, A. V. Prosvirin, H.-H. Zhao and J.-G. Mao, *Eur. J. Inorg. Chem.*, 2004, 3706.
15 J. Telser and R. S. Drago, *Inorg. Chem.*, 1985, **24**, 4765.

